Sensitivity of laboratory based implementations of edge illumination X-ray phase-contrast imaging

P. C. Diemoz, C. K. Hagen, M. Endrizzi, and A. Olivo

Department of Medical Physics and Bioengineering, University College London, WC1E 6BT London, United Kingdom

We present a theoretical and experimental analysis of the angular sensitivity of edge illumination X-ray phase-contrast imaging in its implementation with conventional X-ray sources (sometimes referred to as the "coded-aperture" method). We study how the polychromaticity and finite source dimensions encountered in laboratory-based setups affect the detected signal. We also show that the sensitivity is independent of the period of the masks. Experimental images are presented and analyzed, proving that, despite the simple setup, high angular resolutions of a few hundred nanoradians can be obtained. © 2013 AIP Publishing LLC. [http://dx.doi.org/10.1063/1.4845015]

The edge illumination (EI) X-ray phase-contrast imaging (XPCi) technique was first introduced in the late nineties, by using collimated and monochromatic synchrotron radiation (SR).[1] It was later demonstrated to be efficiently implementable also with the spatially and temporally incoherent radiation produced by conventional X-ray tubes,[2–4] which makes the technique available in standard X-ray laboratories. This sets the basis for a widespread diffusion of XPCi in real-world applications, a goal sought for more than fifteen years now.

The working principles of EI are schematized in Fig. 1. The beam incident on the sample is collimated, typically to a few tens of μm, by a slit set at a distance z_{so} from the source (the "sample aperture," see Fig. 1(a)). The transmitted beam is then analysed by a second slit (the "detector aperture"), placed in front of a row of detector pixels at a distance z_{od} downstream from the object, so as to stop either the lower or the upper part of the beam. The intensity of the beam incident on the detector aperture will be reduced due to sample attenuation, and its spatial position shifted due to refraction produced at the sample interfaces. As a result of the latter, photons previously hitting the detector aperture can be deviated outside it (reducing the counts), or photons previously stopped by the absorbing septa can be deflected into the aperture (increasing the counts). If the sample is scanned through the beam, an image showing a mixture of absorption and refraction contrast is obtained.[5,6] The EI principle can also be applied to the divergent beams provided by conventional X-ray sources if appropriate masks with multiple apertures are employed (Fig. 1(b)). In the latter implementation, the method is also referred to as coded-aperture XPCi.

In recent work we showed that, with highly coherent SR, EI allows achieving unprecedented angular resolution, down to a few nanoradians.[6] The aim of the present work is to study how the sensitivity is affected by the non-ideal conditions (in particular spatial and temporal incoherence) of a laboratory implementation. This is of primary importance in order to assess the potential of the technique in many fields of application.

The EI technique shares some common features with grating interferometry (GI) XPCi[7–9] and other grating non-interferometric XPCi methods,[10] since all these techniques use phase or absorption masks/gratings to perturb and sense the X-ray beam, although the actual working principles and acquisition methods are very different.[11] This similarity can be misleading: in particular, a common misconception is that the EI sensitivity is inversely proportional to the mask period, as in GI.[9,12–14] This would imply a much reduced sensitivity for EI, since it uses periods more than one order of magnitude larger. Besides proving that the sensitivity is independent of the mask period, we analyse the parameters influencing it, in particular the dimensions of the focal spot and the beam polychromaticity. Finally we demonstrate experimentally, by using one of the setups installed at UCL, that high angular sensitivities, comparable to those provided by GI, are obtained.

For simplicity's sake, in the following we consider the "scanning" setup (shown in Fig. 1(a)). This is completely equivalent to the case where multiple apertures are used and the object is static (Fig. 1(b)), provided the mask period is large enough to prevent cross-talk between adjacent apertures (the plurality of beams effectively replaces sample scanning).[15] For a polychromatic beam with energies ranging from E_{min} to E_{max}, the intensity on the detector is simply the sum of all monochromatic components,[6]

$$I_{obj}(x_e;p) = I_0 \int_{E_{min}}^{E_{max}} dE f(E) T(p;E) C(x_e - z_{od}\Delta\theta_x(p;E);E),$$
(1)

where I_0 is the number of photons incident on the sample, $f(E)$ is a normalized weight function taking into account both the beam spectrum and the detector energy response, $T(p;E)$ and $\Delta\theta_x(p;E)$ are the (position and energy dependent) transmission and refraction angle from the object, respectively, and p the position in the object along the direction x. $C(x_e;E) \equiv \int_{x_e}^{x_e+d} dx \rho_{ref}(x;E)$ is the so-called illumination function, where $\rho_{ref}(x;E)$ is the normalized spatial distribution at energy E of the beam incident on the detector mask, in the absence of the sample, x_e is the position of the lower edge of the detector aperture and d the size of the aperture. The shape of $C(x;E)$ depends, in general, on the considered
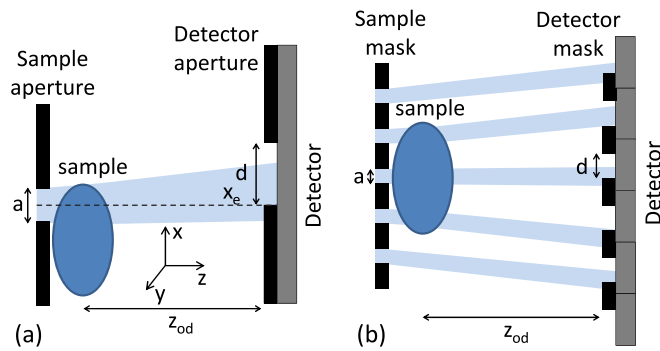
103, 244104-1

FIG. 1. (a) Diagram of the EI principle and (b) of its implementation with divergent beams (not to scale).

energy.[6] However, we will assume that the blurring resulting from the use of an extended source is such that diffraction effects can be neglected (the general polychromatic case is discussed in the supplementary material[16]). The geometrical optics approximation can then be safely used, as demonstrated by Munro *et al.*[17] In this case, it can be shown that the beam shape and the illumination curve are independent from energy, i.e., $\rho_{ref}(x;E) = \rho_{ref}(x)$ and $C(x_e;E) = C(x_e)$. This means that, in the case of an extended source size, the EI setup is achromatic, since the only dependence upon energy is that related to sample attenuation and refraction.

Equation (1) can then be rewritten in a more compact form (by also discarding for simplicity of notation the dependence upon the object coordinate p) as a function of the effective transmission T_{eff} and refraction angle $\Delta\theta_{x,eff}$, obtained by appropriate weighting over the entire spectrum,[11]

$$I_{obj}(x_e) = I_0 T_{eff} C\left(x_e - z_{od}\Delta\theta_{x,eff}\right). \quad (2)$$

Note that the effective energy associated to T_{eff} and $\Delta\theta_{x,eff}$ is in general different (see Munro *et al.*[11] for a detailed analysis on the concept of effective energy in polychromatic XPCi).

Let us now assume that two images of the sample are acquired, with the detector mask set so as to stop a lower ("+" position) or upper ("−" position) portion of the beam. By dividing the two intensities, the dependence upon the object transmission cancels out

$$\frac{I_{obj,+}}{I_{obj,-}} = \frac{C\left(x_{e,+} - z_{od}\Delta\theta_{x,eff}\right)}{C\left(x_{e,-} - z_{od}\Delta\theta_{x,eff}\right)} \equiv R\left(z_{od}\Delta\theta_{x,eff}\right). \quad (3)$$

The function R can be calculated numerically from the experimental measure of the illumination curve or from its theoretical expression. Equation (3) can then be inverted to provide the effective refraction angle

$$\Delta\theta_{x,eff} = \frac{1}{z_{od}} R^{-1}\left(\frac{I_{obj,+}}{I_{obj,-}}\right). \quad (4)$$

The effective object transmission can be derived, instead, by using Eq. (2) and the value for the refraction angle calculated above, i.e.,

$$T_{eff} = \frac{I_{obj,+}}{I_0 C\left(x_{e,+} - R^{-1}\left(\frac{I_{obj,+}}{I_{obj,-}}\right)\right)}. \quad (5)$$

Importantly, Eqs. (4) and (5) also provide a means to estimate analytically the uncertainty on the calculated values T_{eff} and $\Delta\theta_{x,eff}$. In fact, in the approximation of small statistical errors on the input intensities $I_{obj,+}$ and $I_{obj,-}$, and in the special case of symmetric "plus" and "minus" positions, i.e., $C(x_{e,+}) = C(x_{e,-})$, one can write (cf. Eqs. (4) and (5))

$$\sigma\left(\Delta\theta_{x,eff}\right) \simeq \frac{\sqrt{C(x_{e,+})}}{z_{od}\sqrt{2T_{eff}I_0}\left[\rho_{ref}(x_{e,+}) - \rho_{ref}(x_{e,+} + d)\right]}, \quad (6)$$

$$\sigma(T_{eff}) \simeq \frac{\sqrt{3T_{eff}}}{\sqrt{2I_0 C(x_{e,+})}}. \quad (7)$$

Equation (6) is the central result of this analysis. It shows that, in addition to photon statistics and propagation distance, the sensitivity is determined by the chosen level of illumination $C(x_{e,+})$ and by the distribution of the beam incident on the detector mask, which in turn depends on the source dimensions. The mask period does not appear in the expression, which can be easily understood considering that each aperture does not interact with the adjacent ones. Equation (6) represents a generalization of the results obtained in Diemoz *et al.*,[6] in the case of polychromatic spatially incoherent radiation, illumination fractions different from 50% and a detector aperture of finite size.

The variation of the sensitivity as a function of the source full width at half maximum (FWHM, for a Gaussian shaped source) is analyzed in Fig. 2, by considering the parameters of our experimental setup and a detector mask positioned so as to cut half of the beam at both the "−" and "+" positions. The pitch of the sample mask is $66.8\,\mu m$ and the aperture $12\,\mu m$, while the detector mask has pitch and aperture of $83.5\,\mu m$ and $20\,\mu m$, respectively. The setup distances are $z_{so} = 1.6\,m$ and $z_{od} = 0.4\,m$, and the x-ray source is the Rigaku 007HF, using a Mo target and operated at $35\,kV/25\,mA$.

In the first case (blue curve), the sensitivity is obtained by applying Eq. (6) and calculating the beam distribution $\rho_{ref}(x)$ by using the geometrical optics approximation.
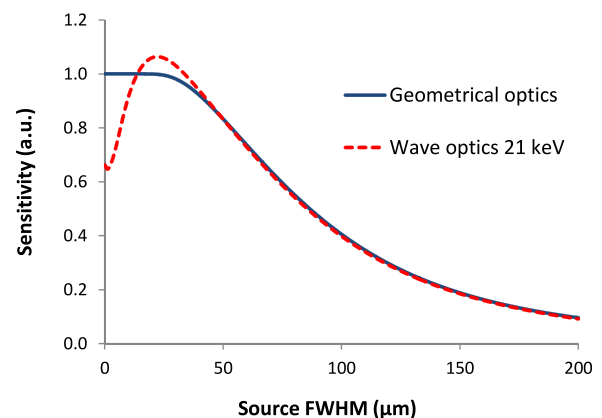

FIG. 2. Variation of the sensitivity as a function of the source dimensions. The following parameters are considered: $a = 12\,\mu m$, $d = 20\,\mu m$, $z_{so} = 1.6\,m$, $z_{od} = 0.4\,m$, corresponding to our experimental setup.

Under this assumption, the beam shape is equal to the blurred projection of the sample aperture at the detector plane. In the second case (red dashed curve), the beam distribution has been calculated using the more accurate wave optics formalism for an energy of 21 keV, corresponding to the refraction effective energy of our system. Figure 2 shows that, for source sizes larger than approximately 45 μm (corresponding to a projected source size of 11 μm), the profiles match, confirming that the beam distribution can be described through the simplified geometrical optics formalism. This is the case encountered in our setup, which features a source FWHM of about 70 μm. For smaller source sizes, diffraction effects are not negligible. In particular, Fig. 2 shows that the sensitivity function is not necessarily monotonously decreasing with the source size: the curve obtained at 21 keV, in fact, has a maximum at around 22 μm. Note that, the diffraction effects being highly energy dependent, other energies would produce different maximum positions (see supplementary material for a more general calculation of the sensitivity curve in the polychromatic case[16]).

Remarkably, both profiles demonstrate that, until approximately 50 μm, an increase in the source size does not lead to an appreciable reduction in the sensitivity. This effect extends to even larger source sizes for different setups based on larger pre-sample apertures, although in that case the starting sensitivity could be lower. Even above this limit, the decrease is slow, indicating that EI-XPCi can be implemented with relatively large source dimensions with negligible loss in the refraction signal. For example, at the source size of 70 μm employed in our experimental setup, the sensitivity is about 66% of the value that would be achieved with a point source.

In the following, we present experimental images obtained with the described EI-XPCi setup, in order to demonstrate its high angular sensitivity. This system has been used over the last years in several experiments,[4,11,18,19] including the imaging of cartilage[18] and breast[19] specimens.

The experimental settings considered in this work are the same as those routinely used for image acquisition, therefore providing an estimate of the system sensitivity under standard operating conditions. The sample mask is made of a series of 720, 4.8 cm long vertical apertures, obtained in a ~30 μm gold layer electroplated on a graphite substrate. The detector mask was produced with a similar design, however it is slightly underplated and the gold thickness is approximately 20 μm, leading to partial transmission through the mask and therefore to a slight reduction in sensitivity. The detector is the ANRAD "SMAM" amorphous selenium flat panel of 85 μm pixel size.

Three different filaments were imaged: 250 μm diameter sapphire, 200 μm diameter boron (with a tungsten core of 14 μm), and 100 μm diameter polyethylene terephthalate (PET). For each of the "+" and "−" positions, 8 dithering steps (with 7 s exposure time) were performed, i.e., 8 images were acquired at different sub-period sample displacements, in order to increase the spatial resolution.[20] The retrieved refraction images are shown in Figs. 3(a)–3(c) and Figs. 3(d)–3(f) for the wires in air and in water, respectively (note that dithering effectively leads to a pixel with asymmetrical dimensions in the two directions, and that a different grayscale has been chosen for the two images; noise is slightly increased in d-f due to the additional absorption of water). Even in the second case all objects are visible, including the PET wire, despite its limited size and the very small refraction angles measured at its edges, of only approximately 0.8 μrad (Fig. 3(h)). As an example, the retrieved refraction profiles for the PET wire in air and in water have been compared with the theoretical ones at the effective energy of 21 keV (Figs. 3(g) and 3(h)), proving the very good quantitative accuracy of the method. Furthermore, following the approach used by Diemoz *et al.*,[6] the system angular resolution has been calculated as the standard deviation of the values in very large (500 × 100 pixels) regions in air. This calculation provided a value of 270 ± 5 nrad, which is also
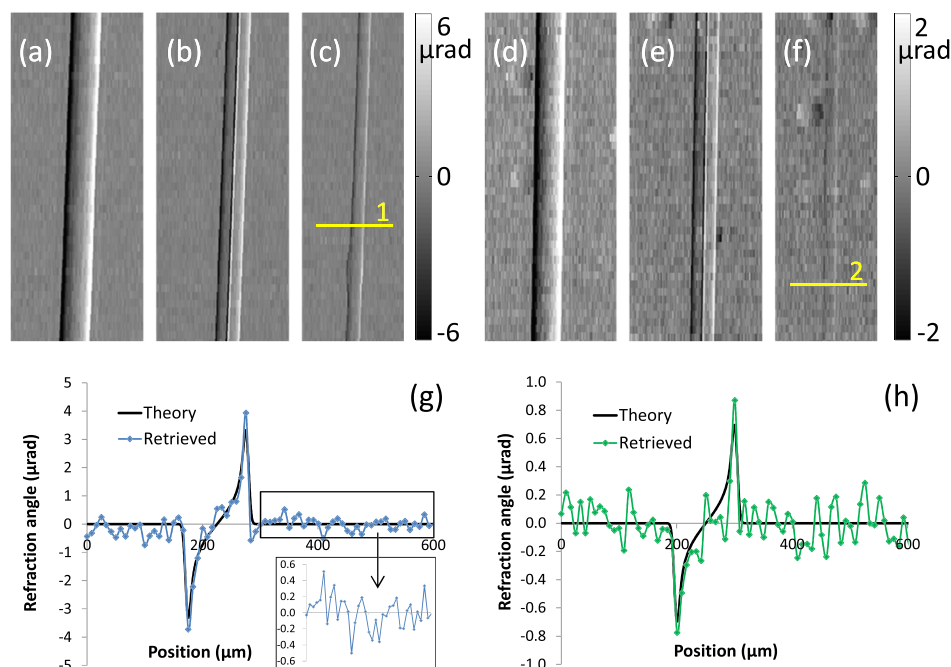

FIG. 3. Retrieved refraction images of three filaments in air: (a) 250 μm sapphire, (b) 200 μm boron with a tungsten core, and (c) 100 μm PET. (d)–f) Same filaments immersed in water. (g,h) Intensity profiles from lines 1 and 2 are plotted against the theoretical refraction angles at 21 keV (the profile in (h) has been averaged over 5 image rows to reduce the noise; the one in (g) comes from a single row).
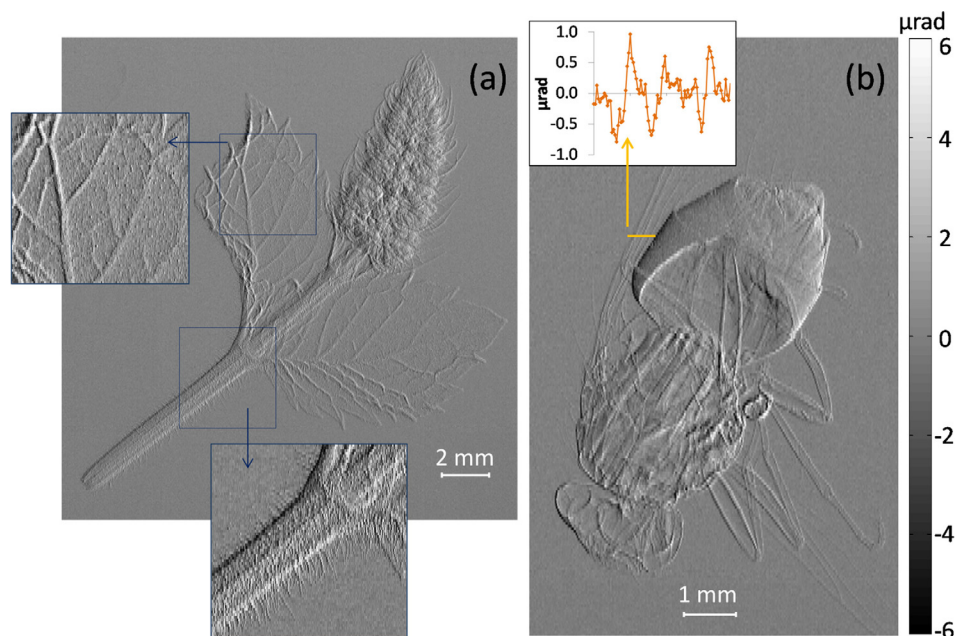
FIG. 4. Refraction images of (a) a mint flower and (b) a fly. Enlarged and contrast-enhanced views of the flower stem and leaf are shown in the insets of (a). A profile across the fly wing (averaged over 5 rows) is shown in the inset of (b).

confirmed by the level of noise visible in the inset of Fig. 3(g).

Comprehensive theoretical and experimental estimations of the sensitivity for the laboratory-based implementation of GI-XPCi were reported in the works of Thüring *et al.*[13,14] and Revol *et al.*[12] Thüring *et al.*[13,14] considered different compact systems employing a microfocus source (FWHM = 5–10 μm). Sixteen images (phase steps) along the GI transmission curve were acquired in order to obtain the refraction image, with an exposure time of 8 s per image (total exposure time 128 s). Measured refraction sensitivities of 250–300 nrad were reported for the Talbot-Lau setups (making use of an additional source grating) and 500–700 nrad for the Talbot setup.[13,14] Revol *et al.*[12] considered a Talbot-Lau setup using an X-ray source of 1 mm focal spot. Twelve phase steps were collected, with an exposure time of 6.7 s per image (total exposure time 80.4 s). Standard deviations down to about 2.5×10^{-3} were obtained for the lateral shift of the transmission curve (Fig. 5 in Ref. 12), from which an angular sensitivity of 110 nrad can be calculated. These results were, however, achieved by using a large number of phase steps along the transmission curve.

Although the layouts of the considered EI and GI systems are different, the obtained values demonstrate that a sensitivity comparable to GI can be reproduced with an EI setup, despite employing masks with periods 15–35 times larger. The use of much larger mask periods and apertures leads to advantages in terms of simplicity of the alignment procedure, increased stability and, not least, simpler manufacturing of masks with large field of view. Our results were obtained with a total exposure time of $2 \times 8 \times 7$ s = 112 s. The same sensitivity, however, would be obtained with only 2 acquired images and 14 s of total exposure when dithering is not needed, as is the case for many biomedical applications[19] (note that dithering does not affect the statistics in each pixel, but only improves the spatial resolution).

In order to further demonstrate the high sensitivity of the technique, we report in Fig. 4 the refraction images obtained for two biological objects: a mint flower and a fly.

The acquisition parameters are the same as those described above. Thanks to the high angular resolution, very fine details are clearly detected in the two samples. Examples are the hairs on the stem of the flower (Fig. 4(a)) and the wings of the fly (Fig. 4(b)), both featuring angles of less than 1 μrad (see inset of Fig. 4(b)). Note that the texture visible in the mint leaf (inset of Fig. 4(a)) is not noise but features of the object only partially resolved by the pixel size. The high image quality achieved also proves the high resilience of the EI technique to mechanical vibrations: despite our setup being installed on the second floor of a highly populated university building, situated in central London close to major roads and above underground lines, no vibration damping was employed.[21]

We have developed a detailed theoretical framework and provided direct experimental validation showing that high refraction sensitivities can be obtained with laboratory-based EI, despite large mask apertures and periods, and the use of uncollimated and unapertured X-ray sources. It should be noted that an even higher sensitivity could have been achieved by using a thicker, totally absorbing detector mask, or by increasing the exposure time, which was kept to a minimum in the measurements.

This high sensitivity, alongside benefits such as achromaticity, relaxed stability requirements, easy alignment and high design flexibility, makes EI-XPCi a strong contender for installation in laboratories worldwide and, ultimately, for translation into "real-world" applications.

[1]A. Olivo, F. Arfelli, G. Cantatore, R. Longo, R. H. Menk, S. Pani, M. Prest, P. Poropat, L. Rigon, G. Tromba, E. Vallazza, and E. Castelli, Med. Phys. **28**, 1610 (2001).

[2]A. Olivo and R. D. Speller, Appl. Phys. Lett. **91**, 074106 (2007).

[3]K. Ignatyev, P. R. T. Munro, D. Chana, R. D. Speller, and A. Olivo, J. Appl. Phys. **110**, 014906 (2011).

[4]P. R. T. Munro, K. Ignatyev, R. D. Speller, and A. Olivo, Proc. Natl. Acad. Sci. U.S.A. **109**, 13922 (2012).

[5]A. Olivo, P. C. Diemoz, and A. Bravin, Opt. Lett. **37**, 915 (2012).

[6]P. C. Diemoz, M. Endrizzi, C. E. Zapata, Z. D. Pešić, C. Rau, A. Bravin, I. K. Robinson, and A. Olivo, Phys. Rev. Lett. **110**, 138105 (2013).

[7]A. Momose, S. Kawamoto, I. Koyama, Y. Hamaishi, K. Takai, and Y. Suzuki, Jpn. J. Appl. Phys., Part 2 **42**, L866–L868 (2003).

[8]F. Pfeiffer, T. Weitkamp, O. Bunk, and C. David, Nat. Phys. **2**, 258–261 (2006).

[9]P. Modregger, B. R. Pinzer, T. Thüring, S. Rutishauser, C. David, and M. Stampanoni, Opt. Express **19**, 18324–18338 (2011).

[10]Z. F. Huang, K. J. Kang, L. Zhang, Z. Q. Chen, F. Ding, Z. T. Wang, and Q. G. Fang, Phys. Rev. A **79**, 013815 (2009).

[11]P. R. T. Munro and A. Olivo, Phys. Rev. A **87**, 053838 (2013).

[12]V. Revol, C. Kottler, R. Kaufmann, U. Straumann, and C. Urban, Rev. Sci. Instrum. **81**, 073709 (2010).

[13]T. Thüring, P. Modregger, S. Hämmerle, S. Weiss, J. Nüesch, and M. Stampanoni, AIP Conf. Proc. **1466**, 293 (2012).

[14]T. Thüring, S. Hämmerle, S. Weiss, J. Nüesch, J. Meiser, J. Mohr, C. David, and M. Stampanoni, Proc. SPIE **8668**, 866813 (2013).

[15]P. R. T. Munro, K. Ignatyev, R. D. Speller, and A. Olivo, Opt. Express **18**, 19681 (2010).

[16]See supplementary material at http://dx.doi.org/10.1063/1.4845015 for a discussion of polychromatic EI in the general case where geometrical optics does not hold.

[17]P. R. T. Munro, K. Ignatyev, R. D. Speller, and A. Olivo, Opt. Express **18**, 4103 (2010).

[18]M. Marenzana, C. K. Hagen, P. Das Neves Borges, M. Endrizzi, M. B. Szafraniec, K. Ignatyev, and A. Olivo, Phys. Med. Biol. **57**, 8173–8184 (2012).

[19]A. Olivo, S. Gkoumas, M. Endrizzi, C. K. Hagen, M. B. Szafraniec, P. C. Diemoz, P. R. T. Munro, K. Ignatyev, B. Johnson, J. A. Horrocks, S. J. Vinnicombe, J. L. Jones, and R. D. Speller, Med. Phys. **40**, 090701 (2013).

[20]K. Ignatyev, P. R. T. Munro, R. D. Speller, and A. Olivo, Rev. Sci. Instrum. **82**, 073702 (2011).

[21]T. P. Millard, M. Endrizzi, K. Ignatyev, C. K. Hagen, P. R. T. Munro, R. D. Speller, and A. Olivo, Rev. Sci. Instrum. **84**, 083702 (2013).